# The C-terminal domain of DNA gyrase A adopts a DNA-bending β-pinwheel fold

**Kevin D. Corbett, Ryan K. Shultzaberger, and James M. Berger***

Department of Molecular and Cellular Biology, 237 Hildebrand Hall 3206, University of California, Berkeley, CA 94720-3206

Edited by Nicholas R. Cozzarelli, University of California, Berkeley, CA, and approved April 2, 2004 (received for review March 8, 2004)

**DNA gyrase is unique among enzymes for its ability to actively introduce negative supercoils into DNA. This function is mediated in part by the C-terminal domain of its A subunit (GyrA CTD). Here, we report the crystal structure of this ≈35-kDa domain determined to 1.75-Å resolution. The GyrA CTD unexpectedly adopts an unusual fold, which we term a β-pinwheel, that is globally reminiscent of a β-propeller but is built of blades with a previously unobserved topology. A large, conserved basic patch on the outer edge of this domain suggests a likely site for binding and bending DNA; fluorescence resonance energy transfer-based assays show that the GyrA CTD is capable of bending DNA by ≥180° over a 40-bp region. Surprisingly, we find that the CTD of the topoisomerase IV A subunit, which shares limited sequence homology with the GyrA CTD, also bends DNA. Together, these data provide a physical explanation for the ability of DNA gyrase to constrain a positive superhelical DNA wrap, and also suggest that the particular substrate preferences of topoisomerase IV might be dictated in part by the function of this domain.**

The topology of cellular DNA is managed by topoisomerases, enzymes that pass DNA strands through each other to relieve excess supercoiling and resolve DNA knots and catenanes (1, 2). Whereas all organisms contain at least one topoisomerase, the bacterium *Escherichia coli* possesses four, each with distinct roles: topoisomerase (topo) I, topo III, topo IV, and DNA gyrase. Topo I and topo III pass single DNA strands through one another to relax negative supercoils (1) or aid RecQ-family helicases in certain DNA repair processes, respectively (3). DNA gyrase and topo IV use ATP to power the transport of one intact DNA duplex through another, an activity that can alter DNA superhelicity as well as promote chromosome decatenation (4, 5).

DNA gyrase and topo IV are members of the type IIA topoisomerase superfamily (6, 7). These enzymes are assembled as oligomeric complexes with distinct domains that coordinate ATP binding and hydrolysis with DNA binding, cleavage, and transport (7, 8). The type IIA topo reaction cycle begins when one segment of DNA, termed the G segment, binds across the central region of the enzyme. ATP binding then triggers a series of motions that leads to the capture of a second DNA duplex (the T segment), cleavage and opening of the G segment, and passage of the T segment through the break. Once the T segment is transported, the G segment is resealed, the T segment is expelled from the protein, and ATP is hydrolyzed and released. This enzymatic cycle alters the linking number of the substrate DNA in discrete steps of ± 2.

Although all type IIA topos share this basic mechanism, there exist distinct type IIA subtypes that have differing substrate specificities and activities. The eukaryotic enzyme, topo II, relaxes positively and negatively supercoiled DNAs at the same rate (9) and can decatenate chromosomes (5). In contrast, most bacteria possess two somewhat more specialized type IIA topos; DNA gyrase and topo IV. Topo IV is found in nearly all bacteria and can both robustly relax positive supercoils and decatenate DNAs, but is much less active on negatively supercoiled substrates (9–11). DNA gyrase, which is found in all bacteria and some archaea, has the unique ability to actively introduce negative supercoils into DNA (4, 12). DNA gyrase function is important for counteracting positive supercoiling forces arising from DNA-unwinding events (13, 14) and for maintaining appropriate levels of supercoiling in the bacterial chromosome (15).

The structural organization of the different type IIA topos also varies. Both bacterial type IIA topos are comprised of two subunits that assemble into $A_2B_2$ heterotetramers, whereas eukaryotic topo IIs fuse the two subunits into a single chain and are homodimeric (6, 7). The bacterial enzymes additionally contain a 30- to 35-kDa domain at the C terminus of their A subunits that is not found in the eukaryotic enzymes. In DNA gyrase subunit A (GyrA), the C-terminal domain (CTD) is thought to bind DNA and help mediate a positive superhelical wrap about the protein (16–19). This wrap allows DNA gyrase to use two closely spaced segments of the same DNA as the G and T segments, first constraining a local positive supercoil, and then inverting it to a negative supercoil upon T segment transport to effect a net change in the linking number of −2 (4, 20). The GyrA CTD is catalytically inactive on its own, but has been shown to independently bind DNA and constrain positive supercoils, and is necessary for DNA gyrase-mediated supercoiling (21). Thus far, any role the CTD might play in the mechanism of the other bacterial type IIA topo, topo IV, has remained unexplored.

Here, we present the crystal structure of the GyrA CTD from the bacterium *Borrelia burgdorferi* (*Bb*Gac). The global architecture of the domain is reminiscent of a β-propeller, but closer inspection reveals a β-strand connectivity and tertiary structure not previously observed in β-propellers. A large fraction of the perimeter of this domain is positively charged, suggesting that DNA might bind and bend around this surface; fluorescence resonance energy transfer (FRET) analysis of the interaction of the GyrA CTD with DNA supports this model. Additionally, sequence alignments show that the CTD of the topo IV A subunit (ParC) is likely to be structurally homologous to the GyrA CTD, and FRET studies show that this domain can also bend DNA. These findings offer a structural explanation for how DNA gyrase is able to introduce negative supercoils into DNA, and reveal an evolutionary and mechanistic connection between the two bacterial type IIA topos.

## Materials and Methods

**Protein Purification.** A construct containing residues 499–810 of *Bb*Gac (corresponding to residues 530–840 of *E. coli* GyrA) was amplified from genomic DNA (American Type Culture Collection), and cloned into a derivative of pET28b with an N-terminal, tobacco etch virus protease-cleavable $His_6$ tag. Protein was

This paper was submitted directly (Track II) to the PNAS office.

Abbreviations: topo, topoisomerase; GyrA, DNA gyrase subunit A; CTD, C-terminal domain; *Bb*Gac, *Borrelia burgdorferi* GyrA CTD; ParC, CTD of the topo IV A subunit; FRET, fluorescence resonance energy transfer.

Data deposition: The atomic coordinates and structure factors have been deposited in the Protein Data Bank, www.pdb.org (PDB ID code 1SUU).

*To whom correspondence should be addressed. E-mail: jmberger@berkeley.edu.

overexpressed in *E. coli* BL21-CodonPlus(DE3)-RIL cells (Stratagene) by inducing with 0.5 mM isopropyl-β-D-thiogalactopyranoside at $OD_{600} = 0.5$ for 4 h at 37°C. Cells were then harvested by centrifugation, resuspended in buffer A (20 mM Hepes, pH 7.5/10% glycerol/2 mM β-mercaptoethanol) plus 800 mM NaCl/10 mM imidazole/50 μg/ml lysozyme, and protease inhibitors, and frozen dropwise into liquid nitrogen.

For purification, cells were sonicated and centrifuged, and the lysate was passed over a $Ni^{2+}$-affinity column (Amersham Biosciences). Peak fractions were pooled, concentrated, and incubated overnight at 4°C with $His_6$-tagged tobacco etch virus protease (22) by using a ratio of 1:50 (wt/wt) tobacco etch virus protease:*Bb*Gac. This mixture was passed over a $Ni^{2+}$-affinity column and the flow-through was further purified over an S-200 gel filtration column (Amersham Biosciences) in buffer A plus 400 mM NaCl, and concentrated by ultrafiltration (Millipore Centriprep-10). Purification of selenomethionine-labeled protein, prepared by the method of Van Duyne *et al.* (23), was performed as for native *Bb*Gac, with the addition of 1 mM Tris(2-carboxyethyl)phosphine (Fluka) in the gel-filtration step and thereafter.

Constructs containing residues 524–841 of *E. coli* DNA gyrase A or residues 497–752 of *E. coli* ParC were cloned and purified for use in FRET assays as described above for *Bb*Gac.

**Crystallization and Structure Determination.** Purified *Bb*Gac at 10–15 mg/ml was dialyzed overnight at 4°C against 20 mM Hepes, pH 7.5 and 300 mM NaCl (plus 1 mM Tris(2-carboxyethyl)-phosphine for selenomethionine-labeled protein). Native crystals were grown in the hanging drop format by mixing 1 μl of protein with 1 μl per well of solution containing 100 mM sodium phosphate buffer (pH 7.4) and 32% polyethylene glycol 3350, and suspending the mixture above well solution diluted 1:1 with water, so that drop equilibration was minimal. To grow large crystals, 0.2 μl of a 1:100 diluted seed stock (prepared by crushing three smaller crystals in 100 μl of crystallization solution) was also added to the drop. Crystals of selenomethionine-labeled protein were grown similarly to native but in microbatch format under Al's Oil (Hampton Research, Aliso Viejo, CA) by using a 1:10 diluted seed stock prepared from native crystals. For harvesting, a cryoprotectant solution containing well solution plus 25% glycerol was added directly to the drop, and the crystals were immediately looped and flash-frozen in liquid nitrogen.

All data sets were collected on Beamline 8.3.1 at the Advanced Light Source at Lawrence Berkeley National Laboratory (Berkeley, CA). Data were indexed and reduced with HKL2000 (24) or ELVES (25) by using MOSFLM (26). Phase calculation was carried out by ELVES using SOLVE (27). Density modification and initial model building was performed by RESOLVE (27), and manual model building was performed with the program O (28). The final model consists of amino acids 506–578, 586–634, and 639–809 of *Bb*Gac; amino acids 506, 527, 543, 578, 648, and 659 are modeled as alanine. A total of 93.2% of non-glycine residues are in the most favored regions of Ramachandran space, and none are in disallowed regions. The model was refined, together with several rounds of manual rebuilding, to a resolution of 1.75 Å, and a final working $R$ factor of 19.4% and an $R_{free}$ of 22.5% (Table 1, which is published as supporting information on the PNAS web site). Refinement was carried out by using REFMAC/ARP (29), followed by TLS refinement (30). Electrostatic surfaces were calculated with GRASP (31), and other figures were produced with PYMOL (32).

**FRET.** Synthetic oligonucleotides 5′-labeled with fluorescein (forward strand) or tetramethylrhodamine (reverse strand) were purchased from Midland Certified Reagents (Midland, TX). The substrates were 40 or 45 bp of a randomly selected segment of pBR322 [positions 3562–3601 (40 bp) or 3606 (45 bp), forward sequence 5′-TAAGTAGTTCGCCAGTTAATAGTTTGCG-CAACGTTGTTGC*CATTG*]. Oligos were purified by using 20% acrylamide/7 M urea gel electrophoresis, recovered by soaking in elution buffer (0.4 M ammonium acetate/10 mM magnesium acetate/1 mM EDTA) overnight, then ethanol-precipitated and resuspended in a small volume of water. Equivalent amounts of complementary oligos were mixed and annealed by placing in a boiling water bath for 5 min, followed by slow cooling to room temperature. Aliquots were snap-frozen and stored at −80°C.

Bending reactions were performed at room temperature in buffer containing 10 mM Hepes pH 7.5, 50 mM KCl, 10% glycerol, and 20 nM oligonucleotide. Higher salt concentrations completely abrogated DNA bending (data not shown). Steady-state fluorescence spectra were taken on a Jobin-Yvon/Horiba Fluoromax-3 spectrofluorometer over a range of wavelengths (FRET $\lambda_{ex} = 490$ nm, $\lambda_{em} = 500–650$ nm; acceptor only $\lambda_{ex} = 560$ nm, $\lambda_{em} = 570–650$ nm). Energy transfer efficiency ($E$) was determined by using the $(\text{ratio})_A$ method and fluorescence readings at 585 nm (33). Data were analyzed by using KALEIDAGRAPH VER. 3.6 (Synergy Software) using a two-state model for DNA bending. This assay directly measures DNA bending and not binding, and it is impossible to determine real dissociation constants for the proteins tested. We could, however, qualitatively compare the relative ability of these proteins to bend DNA. Dye–dye distances ($R$) were estimated by using the equation $E = R_0^6/(R_0^6+R^6)$ (33). A Förster distance ($R_0$) of 50 Å was assumed based on previous studies using this dye pair in similar conditions (34). Models for protein-induced DNA bends were created by using a simple geometric model for DNA of a cylinder 20 Å wide and either 140 Å (40 bp) or 156 Å (45 bp) long, corresponding to ≈4.0 and 4.5 turns of DNA, respectively.

**Structure Prediction.** Sequence alignments and secondary structure predictions were performed by using CLUSTALX (35) and PSI-PRED (36), respectively. Homology models were created with MODELLER (37).

## Results and Discussion

Initial attempts to crystallize the GyrA CTD from *E. coli* were unsuccessful, so we focused instead on the homologous region from *B. burgdorferi*, the causative agent of Lyme disease. Interestingly, the GyrA CTD of *B. burgdorferi* is expressed both independently and as a fusion with the N-terminal domain of GyrA (38). The independently expressed domain is referred to as *Bb*Gac, and consists of amino acids 499–810 of the full-length GyrA protein (39). *In vivo*, *Bb*Gac is present at roughly 4-fold excess over full-length GyrA (38). *B. burgdorferi* possesses a ≈0.9-Mb linear chromosome and up to 17 linear or circular plasmids (40), a complex arrangement that has led to speculation that *Bb*Gac may play a role in the genomic maintenance of this organism (38, 39).

We purified *Bb*Gac from overexpressing *E. coli* cells, and grew crystals of the protein in the space group $P2_12_12_1$, with unit cell dimensions $a = 42.52$ Å, $b = 82.29$ Å, and $c = 88.47$ Å and one chain in the asymmetric unit. We solved the structure by using multiwavelength anomalous diffraction techniques with selenomethionine-labeled protein and refined the resulting model to 1.75-Å resolution. The final model consists of 293 residues with good stereochemistry (Table 1).

**Overall Structure of *Bb*Gac and Implications for β-Propeller Evolution.** The GyrA CTD was predicted previously to adopt a six-bladed β-propeller fold, based on a six-fold tandem repeat in the protein sequence and on secondary structure predictions and threading (Fig. 5, which is published as supporting information on the PNAS web site and ref. 41). Our structure reveals that *Bb*Gac adopts an architecture that is globally reminiscent of a β-pro-

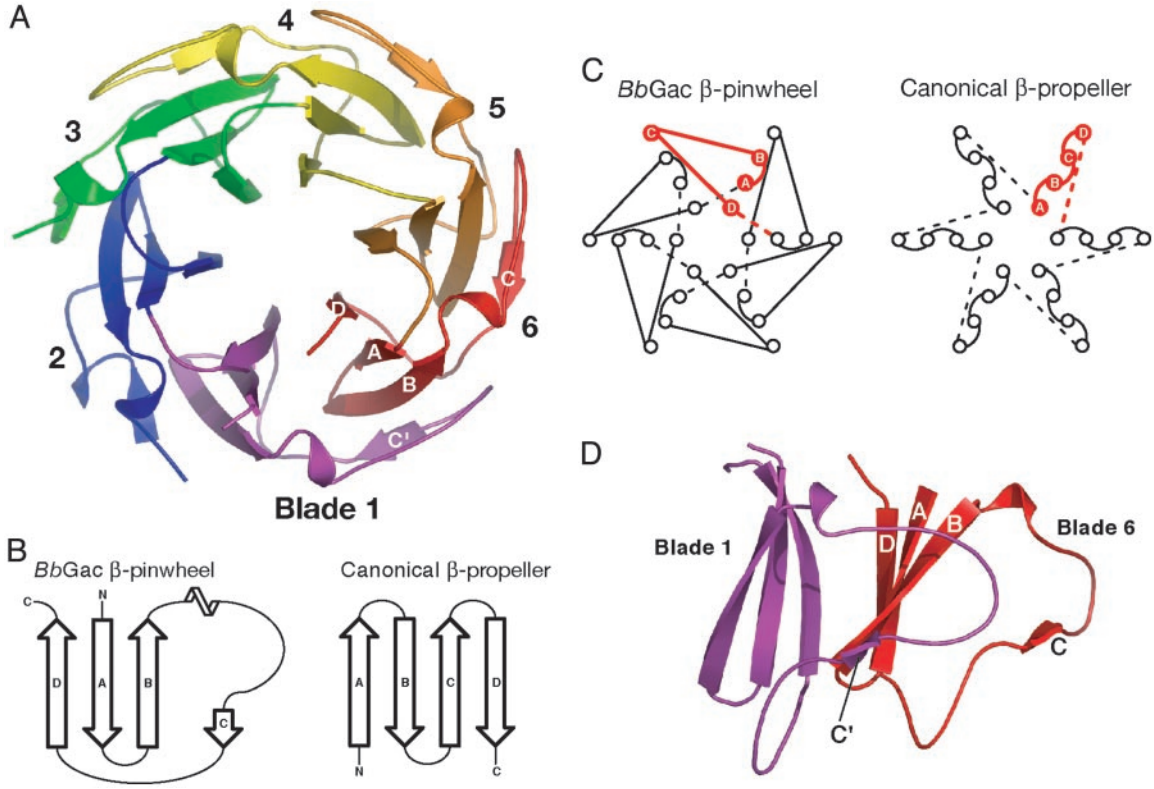


**Fig. 1.** (*A*) Overall structure of *Bb*Gac. Blades 1–6 are purple, blue, green, yellow, orange, and red, respectively. Strands A–D of blade 6 are labeled, as well as strand C of blade 1 (C′). (*B*) Comparison of the strand connectivity within the blades of *Bb*Gac versus a canonical β-propeller. (*C*) Comparison of the overall strand topology between the *Bb*Gac β-pinwheel and a canonical β-propeller. One repeat unit of each is highlighted in red. (*D*) Packing of blades 1 and 6 of *Bb*Gac. Strands A–D of blade 6 are labeled. The C strand of blade 1 (C′) packs against the B strand of blade 6.

peller, with six four-stranded β-sheets arranged in a closed circle (Fig. 1*A*). However, several distinctive features of the *Bb*Gac structure indicate that its fold is unique. Most significantly, the four-strand repeating unit of *Bb*Gac has a topology distinct from that observed in β-propellers (Fig. 1 *B* and *C*). All β-propeller domains solved to date consist of repeating, four-stranded antiparallel hairpin β-sheets with the strand order of A-B-C-D, where A is the innermost and N-terminal strand, and D is the outermost and C-terminal strand (42). In contrast, the repeating units of *Bb*Gac adopt an antiparallel Greek key topology, with an inner-to-outer ordering of D-A-B-C. Another unique property of the *Bb*Gac structure is that each C strand pairs with the B strand of the previous blade, such that each β-sheet is made up of elements from two repeat units (Fig. 1*D*). To accommodate this structure, the loops connecting the B and C strands are quite long, each wrapping around a neighboring blade in the domain (Fig. 1 *A* and *D*). The particular tertiary structure of *Bb*Gac gives the domain a unique pinwheel-type shape, and we propose that it be termed a β-pinwheel fold.

The major families of β-propellers share almost no sequence homology, yet possess an invariant core architecture. As a consequence, it has been debated whether these folds share a common ancestor or instead represent distinct lineages that have converged on this particularly compact structure (42, 43). With the observation of a different blade topology in *Bb*Gac, we conclude that this domain has converged to a propeller-like arrangement independently of other families. It would thus seem that the β-propeller architecture has been "invented" at least twice, supporting the hypothesis that other β-propeller families could also have independently evolved this architecture.

**The GyrA CTD Is Preserved in the Topo IV A Subunit ParC.** In addition to DNA gyrase, most bacteria possess a second type IIA topo (topo IV), which in contrast to gyrase, is unable to supercoil DNA (44). Because of the close sequence homology in their B subunits and in the N-terminal regions of their A subunits, this functional distinction may arise from differences in their A subunit CTDs. In support of this hypothesis, the GyrA CTD is highly conserved among all bacteria, whereas the C-terminal region of the topo IV A subunit ParC is much more variable.

By using our structure of *Bb*Gac, together with standard sequence alignment methods and secondary structure predictions, we aligned the CTDs of ParC proteins with those of GyrA (Fig. 5 and data not shown). This alignment shows not only that the GyrA CTD is largely preserved in most ParC proteins, but also that there are several distinct families of ParC proteins that each possess distinct modifications to the GyrA CTD (Fig. 6, which is published as supporting information on the PNAS web site). One family, from the phylum Firmicutes, possesses a CTD containing all six blades of the β-pinwheel, but appears to be missing the "GyrA box," an ≈8-aa sequence that maps to the long B-C loop on blade 1 of the GyrA CTD and has been noted previously to distinguish GyrA and ParC proteins (45). The second and largest family of ParC proteins, from the phylum Proteobacteria (which includes *E. coli*), possesses a CTD that lacks the GyrA box and also appears to contain only five of the six blades observed in *Bb*Gac. Perhaps most intriguing is a third small family of ParC genes from the phylum Chlamidiae, which appear to be missing the CTD altogether. Previous analyses have suggested that GyrA evolved from ParC, presumably by gaining the CTD and its DNA-wrapping function (46). However, the fact that most ParC proteins contain an altered but related CTD suggests that these enzymes' evolutionary relationships may be more complex than previously thought.

If the CTD is preserved in most ParC proteins but does not

impart supercoiling activity to the enzyme, then what purpose does this region serve for the function of topo IV? It is known that an important and defining characteristic of topo IV is its ability to selectively decatenate and relax positively supercoiled DNAs (10, 11). Single-molecule studies using braided DNA substrates have shown that this selectivity stems from preferential activity on left-handed superhelical DNA crossing (9, 11), a geometry found most often in positively supercoiled DNA (47). In contrast, the eukaryotic topo II shows no specific preference for the DNA-crossing angle (9). Such strong substrate preference appears important for the function of topo IV: its low relaxation rate on negatively supercoiled DNA prevents topo IV from counteracting the negative supercoils created by DNA gyrase, while allowing the enzyme to resolve other, more problematic DNA topologies (10, 11, 15). It seems plausible that the ParC CTD might be partly responsible for the specialized substrate specificity and action of topo IV, directing activity in a manner analogous to the GyrA CTD.

**DNA Bending by the GyrA/ParC CTDs.** DNA gyrase is known from DNase protection and hydroxyl-radical footprinting experiments to bind ≈120–150 bp of DNA, with the central 40–50 bp being more highly protected than the flanking regions (19, 48–52). Because the central region likely corresponds to the ≈35 bp protected by the primary DNA-binding site of other type IIA topos (53, 54), it seems likely that each GyrA CTD binds roughly 40 bp of DNA flanking the G segment. Indeed, studies using the isolated GyrA CTD have shown that it can band-shift small DNAs and also constrain positive supercoils in relaxed DNAs at high protein concentrations (21, 38). Moreover, biochemical assays with *Bb*Gac have further shown that this domain can substitute for the non-sequence-specific architectural protein HU in bacteriophage Mu transposition assays (38). Because HU bends DNA by ≈180° (55), this observation suggests that the GyrA CTD can also significantly distort local DNA structure.

To gain insight into the DNA-binding properties of the GyrA CTD, we inspected the structure for surface regions that might perform this function. The electrostatic surface of *Bb*Gac exhibits an extensive, positively charged region that stretches around approximately two-thirds of the outer edge of the domain, and is formed primarily by the long B-C loops of blades 4, 5, 6, and 1, the latter of which contains the GyrA box motif (Fig. 2). The rest of the *Bb*Gac surface is neutral or negatively charged. Homology models show that the surface charge distribution of *Bb*Gac is likely to be maintained in the *E. coli* GyrA CTD (data not shown), supporting the idea that the large positively charged region might act as a DNA-binding site. Molecular modeling studies suggest that this surface is large enough to bind ≈40 bp of DNA if the nucleic acid is bent significantly around the domain (data not shown).

To directly test whether *Bb*Gac can bend DNA, we performed FRET experiments with end-labeled DNAs. For comparison, we also investigated the properties of the *E. coli* GyrA and ParC CTDs. A 40-bp DNA segment from the plasmid pBR322 was 5′-labeled on opposite strands with fluorescein and tetramethylrhodamine, and FRET efficiencies ($E$ values) were measured over a wide range of protein concentrations. As expected, the isolated DNA displayed an $E$ value of 0.0, indicating a relatively straight overall conformation. Addition of *Bb*Gac significantly increased the FRET efficiency of the DNA substrate ($E$ = 0.43 ± 0.03), consistent with a final dye–dye distance ($R$) of 52 ± 2 Å, and confirming that *Bb*Gac bends DNA (Fig. 3 *A* and *B*). To determine whether the *Bb*Gac footprint on DNA is precisely phased, we tested the domain's ability to bend a DNA segment one-half turn longer than the 40-mer (45 bp). This substrate produced a maximal $E$ value very similar to that of the 40-mer ($E$ = 0.41 ± 0.02 and $R$ = 53 ± 1.5 Å; data not shown), indicating that *Bb*Gac does not bind DNA with any specific phase, and that the measured distances likely represent an average of multiple binding registers.

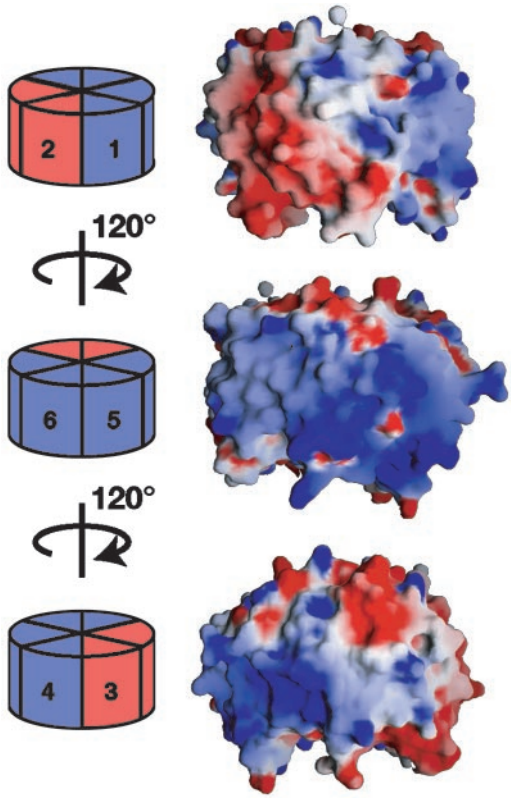


**Fig. 2.** Electrostatic surface representations of *Bb*Gac. The large basic patch (blue) encompasses four blades (1, 4, 5, and 6) and stretches around approximately two-thirds of the outer edge of the domain. The protein orientation and distribution of basic (blue) and acidic (red) regions are shown in schematic diagrams next to each image.

The dye–dye distance obtained by FRET for the 40-mer are consistent with a model in which the CTD smoothly bends DNA around its surface by ≈220 ± 20°. If DNA were wrapped by this amount around a cylinder of fixed radius (*Bb*Gac), one would expect the spacing between the ends of a slightly longer DNA to decrease. However, we see that the dye–dye distance measured for the 40- and 45-mer DNAs are equivalent. This observation can be accounted for by a simple geometric model whereby *Bb*Gac binds DNA over four of its six blades and induces three equally spaced kinks of up to 60° to generate an overall bend of ≈180° (Fig. 3*C*). The use of one or more kinks to bend DNA is not uncommon, and has been observed in several DNA-binding architectural proteins (56).

The isolated *E. coli* GyrA CTD exhibited poor solubility at low salt concentrations, precluding a full analysis of this protein's DNA bending by FRET. However, energy transfer increases were observed at protein concentrations comparable to those assayed for *Bb*Gac, suggesting that results obtained with *Bb*Gac are representative of other GyrA CTDs (data not shown). In contrast, the *E. coli* ParC CTD proved to be well behaved and amenable to analysis. Surprisingly, this domain bent the DNA substrates to nearly the same extent as *Bb*Gac [$E$ = 0.38 ± 0.04 and $R$ = 54 ± 4 Å (40 bp); $E$ = 0.35 ± 0.03 and $R$ = 55 ± 2 Å (45 bp)], although an ≈ 10-fold higher protein concentration was required to observe bending (Fig. 3*B*).

**The Role of the GyrA CTD in Strand Passage by DNA Gyrase.** To better understand how the GyrA CTD might influence DNA gyrase

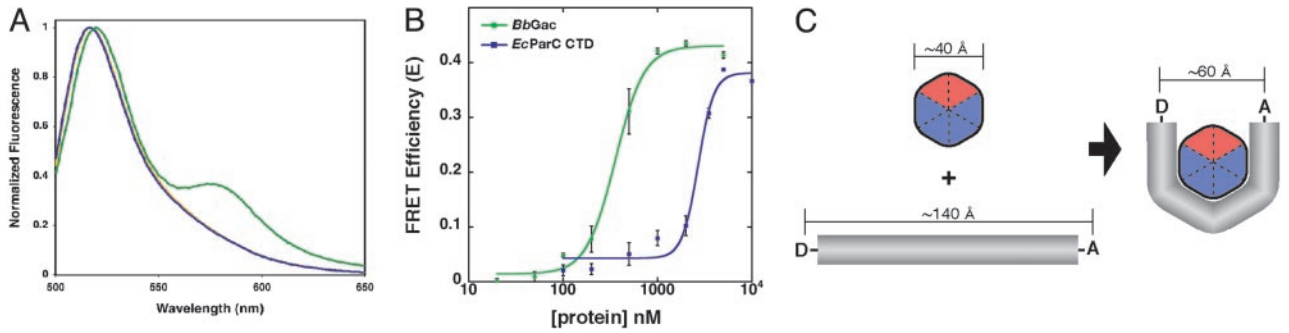


**Fig. 3.** FRET measurements of DNA bending by GyrA and ParC CTDs. (*A*) Representative fluorescence spectra of donor-only-labeled 40-bp duplex DNA (yellow), donor plus acceptor-labeled (blue), and donor plus acceptor-labeled plus 10 $\mu$M *Bb*Gac (green), with maximum donor fluorescence normalized to 1. (*B*) FRET enhancement by *Bb*Gac (green) and *E. coli* ParC CTD (blue), of the 40-bp DNA substrate. (*C*) Schematic view of the GyrA CTD (blue and red) bending a 40-bp DNA substrate labeled with donor (D) and acceptor (A) fluorophores, along with approximate distances involved.

function, we have considered the structure and DNA wrapping ability of the CTD in the context of the holoenzyme. Numerous crystallographic and biochemical studies on various type IIA topo fragments have previously established a general architecture for the minimal catalytic core of these enzymes (Fig. 4*A* and refs. 57–61). To orient the GyrA CTD with respect to the core domains, several pieces of data were taken into account. First, a three-dimensional electron microscopic reconstruction of the intact GyrA dimer revealed the presence of large "lobes" near the top of each GyrA monomer that do not appear to be fully accounted for by the structure of the N-terminal domain alone (60, 62). Second, because there is no significant loss of DNA protection inside the stretch of ≈120–150 bp bound by the enzyme (which includes the bound G segment), the CTD DNA-binding regions are likely to directly flank the primary G-segment-binding site of GyrA. Finally, because the N terminus of the CTD and the C terminus of the N-terminal domain are separated by only a 12- to 15-aa linker, the distance between the two regions is probably less than ≈45 Å.

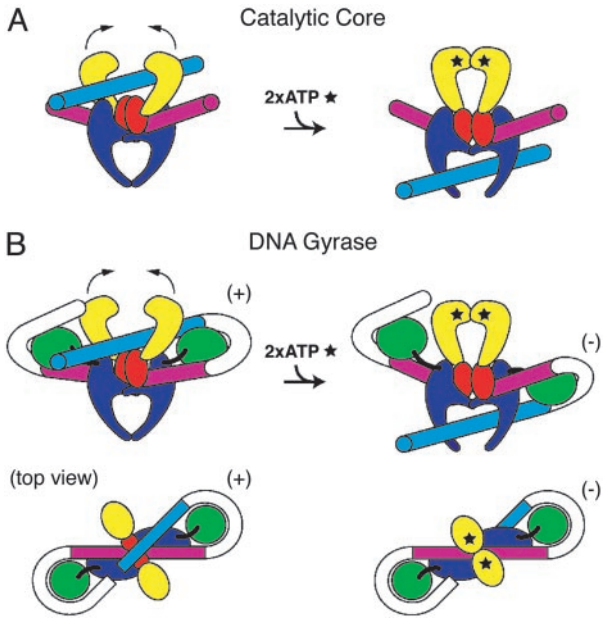


**Fig. 4.** A model for supercoiling by DNA gyrase. Schematic views of strand passage by a type IIA topo catalytic core (no CTD) (*A*) and DNA gyrase (*B*). The DNA-binding/cleavage cores are shown in blue and red, the ATPase domains in yellow, the GyrA CTD in green, and the bound G and T segments in magenta and cyan, respectively. The handedness of the DNA crossover is noted by (+) or (−). We note that a flexible linkage between the N- and C-terminal regions of the A subunit (shown as a black line) might allow the CTD to move with respect to the N-terminal region and thereby help "shuttle" a T segment from one side of the G segment to the other and out of the protein.

A holoenzyme model consistent with these parameters provides a structural mechanism to help explain how DNA gyrase wraps and negatively supercoils DNA (Fig. 4*B*). The DNA regions immediately flanking a G segment, which is centrally bound by the N-terminal region of the A subunit, extend away from the catalytic core where they wrap around the periphery of the CTD. The DNA bending angles we observe by FRET (≥180°) are significant enough to allow each CTD to position its bound DNA between the open jaws of the ATPase domains as a potential T segment, thereby constraining a single positive supercoil with a left-handed superhelical crossover (18, 20, 21, 63). Because the holoenzyme is two-fold symmetric, either GyrA CTD could supply a potential T segment to the ATPase domains, although for strand passage to proceed, only one T segment can be present between the ATPase domains when they dimerize after binding ATP. Once trapped, the T segment can be passed through the cleaved G segment, converting the positive supercoil into a negative supercoil, and altering the linking number by −2.

It is interesting to note that the association of the GyrA CTD with DNA does not appear especially tight (≈500 nM *Bb*Gac is required to fully bend all of the DNA in our FRET assay), and that the linkage between the N- and C-terminal regions may be flexible. As a consequence, the maximal superhelical density achieved by DNA gyrase could reflect a balance between the modest binding energy of the CTD–DNA interaction and the energy required to deform negatively supercoiled DNA into a local positive crossover. The moderate affinity of the CTD for DNA would also allow DNA gyrase to occasionally associate with two distal DNA segments instead of two closely spaced regions of the same DNA, thus permitting this enzyme to catalyze a low level of decatenation (44, 64).

Our model for the function of the GyrA CTD also helps account for certain properties of topo IV. Our data provide direct evidence that the isolated GyrA and ParC CTDs are functionally analogous, suggesting that they may similarly assist DNA recognition and positioning in both enzymes. A major difference between DNA gyrase and topo IV, however, is that topo IV is unable to negatively supercoil DNA. Because the ParC CTD bends DNA less efficiently than the GyrA CTD, it is possible that this domain cannot actively manipulate substrate DNA conformation to the same degree as the GyrA CTD. Rather, this domain might merely assist a productive strand-passage event only when topo IV binds to left-handed superhelical crossovers, possibly accounting for the observed substrate specificity of this enzyme (9, 11).

In summary, the structure of the CTD of DNA gyrase A has proven informative in a number of contexts. The structure provides an example of a specialized $\beta$-propeller-like topology that acts as a DNA-binding and -bending element. These findings in turn have allowed us to construct mechanistic models that account for both the ability of DNA gyrase to wrap and negatively supercoil DNA, and for topo IV to act principally on positively supercoiled and catenated DNAs. In addition, we have uncovered several families of ParC proteins that each possess different variants of the GyrA CTD. In all, our results highlight the emerging idea that distinct type IIA topo subtypes, while globally similar in function, have each been exquisitely tuned by evolution for distinct cellular tasks.

We thank J. Tanamachi and J. Holton for assistance at Advanced Light Source Beamline 8.3.1; D. S. Classen for critical reading of the manuscript; A. Edelstein and D. Theobald for help collecting and analyzing FRET data; S. Marqusee for use of the spectrofluorometer and for helpful discussions; T. Alber and J. Erzberger for helpful discussions; and A. Antczak and M. Price for help with initial work on the *E. coli* GyrA CTD. This work was supported by National Cancer Institute Grant CA 77373 (to J.M.B.). K.D.C is an National Science Foundation Graduate Research Fellow.

1. Champoux, J. J. (2001) *Annu. Rev. Biochem.* **70,** 369–413.
2. Wang, J. C. (2002) *Nat. Rev. Mol. Cell Biol.* **3,** 430–440.
3. Hickson, I. D. (2003) *Nat. Rev. Cancer* **3,** 169–178.
4. Brown, P. O. & Cozzarelli, N. R. (1979) *Science* **206,** 1081–1083.
5. Liu, L. F., Liu, C. C. & Alberts, B. M. (1980) *Cell* **19,** 697–707.
6. Corbett, K. D. & Berger, J. M. (2004) *Ann. Rev. Biophys. Biomol. Struct.* **33,** 95–118.
7. Wang, J. C. (1998) *Q. Rev. Biophys.* **31,** 107–144.
8. Berger, J. M. & Wang, J. C. (1996) *Curr. Opin. Struct. Biol.* **6,** 84–90.
9. Charvin, G., Bensimon, D. & Croquette, V. (2003) *Proc. Natl. Acad. Sci. USA* **100,** 9820–9825.
10. Crisona, N. J., Strick, T. R., Bensimon, D., Croquette, V. & Cozzarelli, N. R. (2000) *Genes Dev.* **14,** 2881–2892.
11. Stone, M. D., Bryant, Z., Crisona, N. J., Smith, S. B., Vologodskii, A. V., Bustamante, C. & Cozzarelli, N. R. (2003) *Proc. Natl. Acad. Sci. USA* **100,** 8654–8659.
12. Gellert, M., Mizuuchi, K., O'Dea, M. H. & Nash, H. A. (1976) *Proc. Natl. Acad. Sci. USA* **73,** 3872–3876.
13. Liu, L. F. & Wang, J. C. (1987) *Proc. Natl. Acad. Sci. USA* **84,** 7024–7027.
14. Zechiedrich, E. L. & Cozzarelli, N. R. (1995) *Genes Dev.* **9,** 2859–2869.
15. Zechiedrich, E. L., Khodursky, A. B., Bachellier, S., Schneider, R., Chen, D., Lilley, D. M. & Cozzarelli, N. R. (2000) *J. Biol. Chem.* **275,** 8103–8113.
16. Reece, R. J. & Maxwell, A. (1989) *J. Biol. Chem.* **264,** 19648–19653.
17. Reece, R. J. & Maxwell, A. (1991) *J. Biol. Chem.* **266,** 3540–3546.
18. Liu, L. F. & Wang, J. C. (1978) *Proc. Natl. Acad. Sci. USA* **75,** 2098–2102.
19. Liu, L. F. & Wang, J. C. (1978) *Cell* **15,** 979–984.
20. Kampranis, S. C., Bates, A. D. & Maxwell, A. (1999) *Proc. Natl. Acad. Sci. USA* **96,** 8414–8419.
21. Reece, R. J. & Maxwell, A. (1991) *Nucleic Acids Res.* **19,** 1399–1405.
22. Kapust, R. B. & Waugh, D. S. (1999) *Protein Sci.* **8,** 1668–1674.
23. Van Duyne, G. D., Standaert, R. F., Karplus, P. A., Schreiber, S. L. & Clardy, J. (1993) *J. Mol. Biol.* **229,** 105–124.
24. Otwinowski, Z. & Minor, W. (1997) *Methods Enzymol.* **276,** 472–494.
25. Holton, J. & Alber, T. (2004) *Proc. Natl. Acad. Sci. USA* **101,** 1537–1542.
26. Leslie, A. G. W. (1992) *Joint CCP4 + ESF-EAMCB Newsletter on Protein Crystallography* No. 26.
27. Terwilliger, T. (2004) *J. Synchrotron. Radiat.* **11,** 49–52.
28. Jones, T. A. & Kjeldgaard, M. (1997) *O-The Manual, Version 7.0* (Uppsala Software Factory, Uppsala).
29. Lamzin, V. S. & Wilson, K. S. (1993) *Acta Crystallogr. D.* **49,** 129–147.
30. Winn, M. D., Isupov, M. N. & Murshudov, G. N. (2001) *Acta Crystallogr. D* **57,** 122–133.
31. Nicholls, A., Sharp, K. A. & Honig, B. (1991) *Proteins Struct. Funct. Genet.* **11,** 281–296.
32. DeLano, W. L. (2002) *Pymol* (DeLano Scientific, San Carlos, CA).
33. Clegg, R. M. (1992) *Methods Enzymol.* **211,** 353–388.
34. Stuhmeier, F., Welch, J. B., Murchie, A. I., Lilley, D. M. & Clegg, R. M. (1997) *Biochemistry* **36,** 13530–13538.
35. Jeanmougin, F., Thompson, J. D., Gouy, M., Higgins, D. G. & Gibson, T. J. (1998) *Trends Biochem. Sci.* **23,** 403–405.
36. Jones, D. T. (1999) *J. Mol. Biol.* **292,** 195–202.
37. Sali, A. & Blundell, T. L. (1993) *J. Mol. Biol.* **234,** 779–815.
38. Knight, S. W. & Samuels, D. S. (1999) *EMBO J.* **18,** 4875–4881.
39. Knight, S. W., Kimmel, B. J., Eggers, C. H. & Samuels, D. S. (2000) *J. Bacteriol.* **182,** 2048–2051.
40. Fraser, C. M., Casjens, S., Huang, W. M., Sutton, G. G., Clayton, R., Lathigra, R., White, O., Ketchum, K. A., Dodson, R., Hickey, E. K., *et al.* (1997) *Nature* **390,** 580–586.
41. Qi, Y., Pei, J. & Grishin, N. V. (2002) *Proteins* **47,** 258–264.
42. Paoli, M. (2001) *Prog. Biophys. Mol. Biol.* **76,** 103–130.
43. Jawad, Z. & Paoli, M. (2002) *Structure (London)* **10,** 447–454.
44. Ullsperger, C. & Cozzarelli, N. R. (1996) *J. Biol. Chem.* **271,** 31549–31555.
45. Ward, D. & Newton, A. (1997) *Mol. Microbiol.* **26,** 897–910.
46. Gadelle, D., Filee, J., Buhler, C. & Forterre, P. (2003) *BioEssays* **25,** 232–242.
47. Vologodskii, A. & Cozzarelli, N. R. (1996) *Biophys. J.* **70,** 2548–2556.
48. Klevan, L. & Wang, J. C. (1980) *Biochemistry* **19,** 5229–5234.
49. Fisher, L. M., Mizuuchi, K., O'Dea, M. H., Ohmori, H. & Gellert, M. (1981) *Proc. Natl. Acad. Sci. USA* **78,** 4165–4169.
50. Kirkegaard, K. & Wang, J. C. (1981) *Cell* **23,** 721–729.
51. Morrison, A. & Cozzarelli, N. R. (1981) *Proc. Natl. Acad. Sci. USA* **78,** 1416–1420.
52. Orphanides, G. & Maxwell, A. (1994) *Nucleic Acids Res.* **22,** 1567–1575.
53. Peng, H. & Marians, K. J. (1995) *J. Biol. Chem.* **270,** 25286–25290.
54. Lee, M. P., Sander, M. & Hsieh, T. (1989) *J. Biol. Chem.* **264,** 21779–21787.
55. Swinger, K. R., Lemberg, K. M., Zhang, Y. & Rice, P. A. (2003) *EMBO J.* **22,** 3749–3760.
56. Bewley, C. A., Gronenborn, A. M. & Clore, G. M. (1998) *Ann. Rev. Biophys. Biomol. Struct.* **27,** 105–131.
57. Berger, J. M., Gamblin, S. J., Harrison, S. C. & Wang, J. C. (1996) *Nature* **379,** 225–232.
58. Classen, D. S., Olland, S. & Berger, J. M. (2003) *Proc. Natl. Acad. Sci. USA* **100,** 10629–10634.
59. Fass, D., Bogden, C. E. & Berger, J. M. (1999) *Nat. Struct. Biol.* **6,** 322–326.
60. Morais Cabral, J. H., Jackson, A. P., Smith, C. V., Shikotra, N., Maxwell, A. & Liddington, R. C. (1997) *Nature* **388,** 903–906.
61. Wigley, D. B., Davies, G. J., Dodson, E. J., Maxwell, A. & Dodson, G. (1991) *Nature* **351,** 624–629.
62. Kirchhausen, T., Wang, J. C. & Harrison, S. C. (1985) *Cell* **41,** 933–943.
63. Rau, D. C., Gellert, M., Thoma, F. & Maxwell, A. (1987) *J. Mol. Biol.* **193,** 555–569.
64. Marions, K. J. (1987) *J. Biol. Chem.* **262,** 10362–10368.